

# The phase of a degenerate Fermi gas

Giovanni Pecci,<sup>1</sup> Piero Naldesi,<sup>1</sup> Anna Minguzzi,<sup>1</sup> and Luigi Amico<sup>2,3,4</sup>

<sup>1</sup>*Univ. Grenoble Alpes, CNRS, LPMMC, 38000 Grenoble, France*

<sup>2</sup>*Quantum Research Centre, Technology Innovation Institute, Abu Dhabi, UAE*

<sup>3</sup>*Centre for Quantum Technologies, National University of Singapore, 3 Science Drive 2, Singapore 117543, Singapore*

<sup>4</sup>*LANEF Chaire d'excellence, Univ. Grenoble-Alpes & CNRS, F-38000 Grenoble, France*

In quantum mechanics, each particle is described by a complex valued wave function characterized by amplitude and phase. When many particles interact each other, cooperative phenomena give rise to a quantum many-body state with a specific quantum coherence. What is the interplay between particle's phase coherence and many-body quantum coherence? Over the years, such question has been object of profound analysis in quantum physics. Here, we demonstrate how state of the art quantum technology allows to explore the question operatively. To this end, we study the time-dependent interference formed by releasing an interacting degenerate Fermi-gas from a specific matter-wave circuit in an effective magnetic field. Particle phase coherence, indicated by the first-order correlator, and many-body quantum coherence, indicated by the noise correlator, are displayed as distinct features of the interferogram. Particle phase coherence produces spiral interference of the Fermi orbitals at intermediate times. Many-body quantum coherence emerges at long times. The coupling between particles coherence and many-body coherence is reflected in a specific dependence of the interference pattern on the effective magnetic field.

**Introduction.** Phase coherence is the ability of the quantum wave-function to retain its phase information. For free particles, such notion is operatively inferred, for example, through the interference pattern in two slits experiments. When it comes to be referred to interacting quantum many particles systems, though, the notion of phase coherence is more involved. While the 'single particle coherence' can cooperate to establish a macroscopic coherence due to the off-diagonal long range order[1], a difference emerges from particle statistics. Bosonic systems can condense and be described by a macroscopic wave function  $\Phi \sim e^{i\phi}$ , with a phase  $\phi$  coinciding with the single-particle phase. For fermionic systems, instead, the Pauli principle hinders the occupancy of a single quantum level by particles with the same spin, and therefore the many-body coherence can be achieved from the single particles' coherence through a more complicated path. On one hand, a frictionless flow, the persistent current, occurring in metallic or superconducting small rings provides a characteristic trait of particle's coherence[2–4]. On the other hand, interacting fermions can define coherent phases of matter, with off-diagonal long range order and specific features of collective excitations[5]. We shall see that persistent currents and off-diagonal long range order in an interacting fermionic gas are indeed intertwined.

With the advent of ultracold atoms quantum technology, quantum coherent bosonic/fermionic systems have been studied with unprecedented degree of control and precision of physical conditions. Although cold atoms systems are made of large but finite number of particles ( $\sim 10^5$ ), 'two slit' tests for a Bose-Einstein Condensate (BEC) provide a meaningful interference pattern as a result of self-averaging[6, 7]. Fundamental limits on fringes visibility are provided by phase diffusion [8, 9]. Bose

Josephson effect is a direct test for BEC coherence[10–13]. The nature of the phase coherence in degenerate fermions depends on particles interaction that can be tuned in cold atoms quantum technology from repulsive to attractive cases[14]. For repulsive interactions, the effects of the ferromagnetic correlations were observed [15, 16]. For attractive interactions, bound states of Fermi pairs can condense, experiencing the BCS-BEC crossover[17]. Relevant information on the system coherence in the crossover can be extracted through the study of the Josephson effect[18–20].

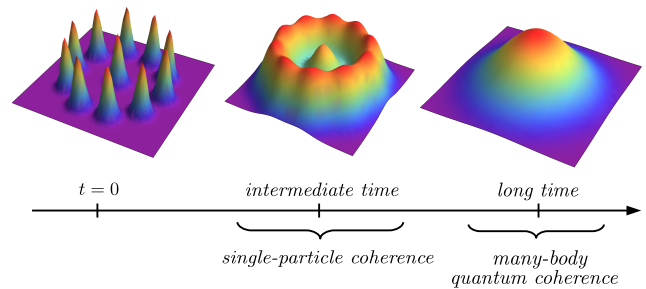


FIG. 1. Expansion protocol at different times. After the release of the trap, the particles in the center and on the ring interfere. We shall see the single-particle coherence to emerge at intermediate times, while in the long-time limit this protocol provides information about the many-body quantum coherence.

In this paper, we explore the phase portrait of the Fermi field in the different circumstances of particles' interactions. For bosonic condensates, the problem has been analysed recently through a series of interferometric experiments (heterodyne phase detection protocol)[21–

23], within the emerging field of atomtronics[24]. The superfluid nature of the system manifests in the quantization of the particles angular momentum (or current). In the heterodyne phase detection protocol a circulating current yields the formation of characteristic spiral interferograms[22, 23].

A specific relation exists between quantized persistent currents and the topological features of the spiral, with relevant differences for repulsive/attractive interactions [22, 25, 26]. The spiral interferograms are washed out by attractive interactions because of the formation of soliton-like ground states[27].

Here, we analyse the interplay between the quantum coherence of each single particle and the interaction effects leading to a many-body quantum coherence. To this end, in analogy with bosonic protocols, we study a degenerate interacting Fermi gas confined in a ring-shaped potential and pierced by an effective magnetic flux. Because of the effective magnetic flux, a current is imprinted on the degenerate gas. Such system is let to interfere with a second gas placed at the center of the ring. The proposed protocol provides a step forward towards the realization of the full counting statistics for the system's particle density fluctuations[28, 29]. Despite the similarity in the schemes, we shall see that the fermionic interferograms are markedly different from the bosonic ones. We shall see that our scheme allows to probe the nature of the one-body phase coherence as well as the many-body quantum coherence in a single protocol.

**Methods.** We consider a gas of  $N$  degenerate fermions confined in a lattice ring comprised of  $N_s$  sites and pierced by an effective magnetic flux induced by an artificial gauge field. Such effective magnetic flux can be applied in several ways, for example by stirring the condensate, by phase imprinting or by two-photon Raman transitions [30]. The system is described by the Hubbard Hamiltonian in a one-dimensional ( $1d$ ) ring-shaped spatial geometry

$$\hat{H}_{FH} = -J \sum_{j=1}^{N_s} \sum_{\sigma=\uparrow,\downarrow} \left( e^{i\tilde{\Omega}} c_{j,\sigma}^\dagger c_{j+1,\sigma} + H.c. \right) + U \sum_{j=1}^{N_s} n_{j,\uparrow} n_{j,\downarrow} \quad (1)$$

where  $U$  is the particles interaction and  $J$  is the tunnel amplitude. The applied gauge field is taken into account through the Peierls phase factors  $e^{i\tilde{\Omega}}$ , in which  $\tilde{\Omega} \doteq \frac{2\pi}{N_s} \frac{\Omega}{\Omega_0}$ , with  $\Omega_0$  being the flux quantum.

For  $U > 0$ , the Hubbard ground state many-body wavefunction is made of extended states characterized by real wave momenta[31]. For  $U < 0$ , the ground state is characterized by bound pairs, with complex wave momenta. For weak attractions, the ground state of the system is a BCS-like state with the wavefunction of the pair decaying on distance larger than the mean interparticle separation[32–34]. For stronger attractions, the bound states are formed by tightly bound particle pairs.

The persistent currents in Hubbard models for repul-

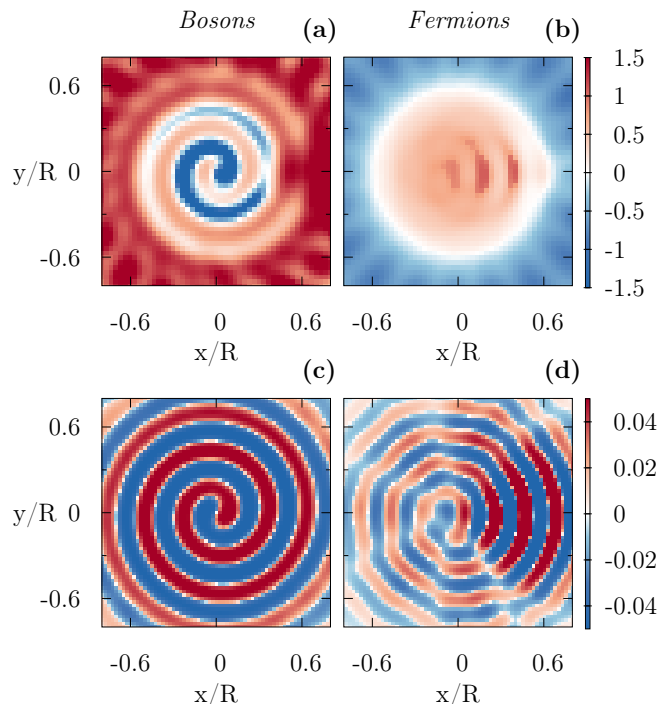


FIG. 2. Intermediate times density-density correlations. The Bose and the Fermi case are compared. In the upper panels, the overall correlation  $G(\mathbf{r}, \mathbf{r}', t)$  for  $\omega_0 t = 3$  is presented. In (c) and (d), the interference  $\tilde{G}^{C,R}(\mathbf{r}, \mathbf{r}', t)$  between the ring and the central site is displayed (see also text). Calculation performed by DMRG on a system of  $N = 14$  particles on  $N_s = 20$  sites, with interaction  $U/J = 0.2$  and  $\tilde{\Omega} = 1.4$ .

sive interactions was studied in [35] and very recently in Ref.[36] for attractive interactions. We note that continuous ring-shaped fermions with delta-interaction can be achieved from Hubbard rings in the small fillings  $N/N_s$  regimes (see Supplementary information).

Inspired by the protocol employed for bosonic systems, we study the dynamics of the co-expansion of the ring-shape degenerate gas with a free fermionic gas located at the ring's centre. In the experiment with weakly interacting bosonic condensates, the spiral interferogram emerges in a single co-expansion. In our theoretical approach, however, the particle density is reconstructed as an expectation value on different instances of the co-expansion protocols:  $\rho(\mathbf{r}, t) \doteq \sum_{\alpha=\uparrow,\downarrow} \langle \Psi_\alpha(\mathbf{r}, t)^\dagger \Psi_\alpha(\mathbf{r}, t) \rangle$ , being  $\Psi_\alpha(\mathbf{r}, t) = \sum_j w_j(\mathbf{r}, t) c_{j,\alpha}$  the field operator of the whole system (ring plus centre) and  $w_j$  Wannier functions. Since each co-expansion is characterized by a well defined, yet randomly distributed, relative phase between the ring gas and the central system, the system's phase pattern is washed out in  $\rho(\mathbf{r}, t)$ [37]. We shall see, instead, that non trivial phase informations on the system are captured by the density-density correlator:  $G(\mathbf{r}, \mathbf{r}'; t) \doteq \sum_{\alpha,\beta=\uparrow,\downarrow} G_{\alpha,\beta}(\mathbf{r}, \mathbf{r}'; t)$ , where  $G_{\alpha,\beta}(\mathbf{r}, \mathbf{r}'; t) \doteq \langle \Psi_\alpha(\mathbf{r}, t)^\dagger \Psi_\alpha(\mathbf{r}, t) \Psi_\beta(\mathbf{r}', t)^\dagger \Psi_\beta(\mathbf{r}', t) \rangle$ . For our combined

centre-ring system, such correlation can be broken down as  $G(\mathbf{r}, \mathbf{r}', t) = G^{(C,C)} + G^{(R,R)} + G^{(C,R)}$ . Since ring and central gases are disconnected until the traps are lifted,  $|\psi(t=0)\rangle = |\psi(t=0)\rangle_c \otimes |\psi(t=0)\rangle_{ring}$ . Assuming a free expansion for  $t \geq 0$ , the ring-centre correlations read  $G^{(C,R)}(\mathbf{r}, \mathbf{r}', t) = \rho^{(R)}(\mathbf{r}, t)\rho^{(C)}(\mathbf{r}', t) + \rho^{(R)}(\mathbf{r}', t)\rho^{(C)}(\mathbf{r}, t) + \tilde{G}^{(C,R)}(\mathbf{r}, \mathbf{r}', t)$ , where

$$\tilde{G}^{(C,R)}(\mathbf{r}, \mathbf{r}', t) = \sum_{\alpha, \beta} \sum_{i, j} I_{i, j}(\mathbf{r}, \mathbf{r}', t) \delta_{\alpha, \beta} \left( \delta_{ij} - \langle c_{i, \alpha}^\dagger c_{j, \alpha} \rangle \right) \quad (2)$$

with  $I_{ij}(\mathbf{r}, \mathbf{r}', t) \doteq w_C^*(\mathbf{r}, t)w_C(\mathbf{r}', t)w_j^*(\mathbf{r}, t)w_j(\mathbf{r}', t)$ . From Eq. (2) we see that the interference between the center and the ring only affects particle belonging to the same spin species. We note that such correlation can be accessed by measuring separately the full correlator  $G(\mathbf{r}, \mathbf{r}')$  and the exceeding terms depending on densities only.

In our approach, we monitor the complete correlator  $G(\mathbf{r}, \mathbf{r}', t)$ , the interference term  $\tilde{G}^{(C,R)}$  Eq. (2) and the spin resolved correlator  $G_{\uparrow, \downarrow}$ . In our analysis, the time scale for expansion is taken as the inverse of the single lattice well frequency  $\omega_0$ . We shall see that at intermediate times  $\tilde{G}^{(C,R)}$  contains direct information on the single-particle phase coherence.

Instead, at long times,  $G_{\uparrow, \downarrow}(\mathbf{r}, \mathbf{r}', t)$  probes the many-body phase coherence in momentum space with  $\mathbf{k} = m\mathbf{r}/\hbar t_{exp}$ ,  $\mathbf{k}' = m\mathbf{r}'/\hbar t_{exp}$ .

In the present paper we use a DMRG analysis of the correlator matrix. For a lattice with  $N_s$  sites, the calculation of  $N_s^4$  correlators are required to be accessed.

**Bosons Vs Fermions.** For bosons, the spiral interference pattern arises because of the simple coupling between the effective gauge field and the phase of the Bose condensate. The quantized circulation reflects the effective magnetic flux quantization. The complete phase structure of the bosonic field emerges as a characteristic spiral interferogram in the expanding density [21–23] as well as in the noise correlator  $G(\mathbf{r}, \mathbf{r}'; t)$ [37] (see Fig. 2 c).

For fermionic systems, the relation between the imparted phase and the momentum distribution is more involved. The difference traces back to the symmetry properties of the many-body wave functions of the two systems resulting in a different momentum distribution: while bosonic wave functions yield a momentum distribution peaked at  $k = 0$ [38–40], Fermi systems are characterized by a broader momentum distribution. Then, when fermionic particles are put in motion by an effective magnetic flux each momentum component of the distribution is characterized by a different phase factor. As a consequence, phases recombination occurs, and the time of flight image of the density results to be suppressed at  $|\mathbf{k}| = 0$  only after half of the Fermi sphere is displaced by the effective magnetic flux (see Supplementary information). Correspondingly, in the  $G(\mathbf{r}, \mathbf{r}'; t)$  at intermediate expansion times, the different momenta character-

ize distinct particle orbitals (see Fig.2 d). For  $U = 0$ , such orbitals are strictly single-particle (see Supplementary material). We find that for each orbital a spiral-like interference emerges. In addition, specific dislocations are found in the interference pattern at which the particle density is suppressed. Such dislocations, just  $N_\uparrow - 1$  (or equivalently  $N_\downarrow - 1$ ) in number, are due to the interference of the  $N_\uparrow(N_\downarrow)$  independent orbitals. Remarkably, the dislocations are clearly visible at small and moderate interactions. By increasing interactions, we find such feature disappears indicating that the system cannot be described in terms of independent quasi-particles.

**Repulsive Vs Attractive interactions.** Below, we demonstrate that the long time expansion of our protocol's interference allows us to access to many-body coherence through the noise correlator (see also Supplementary Material). We shall see that the different nature of many-body state for repulsive and attractive interactions is clearly reflected in our pictures (see Fig. 3).

For  $U > 0$  the ground state of the system is made of itinerant correlated particles. Therefore, the interferograms reflect the phase pattern imparted by the effective magnetic flux putting the system in a coherent motion. By the analysis of the long-time behavior of  $G_{\uparrow, \downarrow}(\mathbf{r}, \mathbf{r}'; t)$ , at increasing  $U$  we find that the correlation has a clear symmetry  $k = k'$  (see the caption of Fig. 3), reflecting the system's tendency to magnetic ordering occurring at large  $U/J$ [41]. As function of the applied effective magnetic flux, the correlations are found to be displaced by a discrete amount reflecting the quantized particle circulation.

For  $U < 0$ , the system is characterized by the off-diagonal (quasi) long-range order due to fermionic pairing [1]. In contrast with repulsive cases, for  $U < 0$  we found that the correlator  $G(\mathbf{r}, \mathbf{r}'; t)$  displays a marked structure along the whole anti-diagonal  $x = -x'$ , reflecting the formation of pairs of smaller and smaller size at increasing  $|U|$ : while in the BCS regime the pairs correspond to enhanced  $(\mathbf{k}_F, -\mathbf{k}_F)$  correlations at the Fermi sphere i.e. for wave vector  $|\mathbf{k}| = k_F$ , at larger interactions, where pairs of small spatial size are formed, correlations along the whole antidiagonal  $(\mathbf{k}, -\mathbf{k})$  are predicted. Such approach is in line with [29, 42] and further analysed in the Supplementary material. Despite our system can be of small size, the antidiagonal correlations features clearly emerge in our expansion protocol (at long times), thus allowing to probe the nature of pairing in the whole BCS-BEC crossover. For attractive or repulsive interactions, we find that the landscape along the anti-diagonal depends on the number of particles with a markedly different scaling for  $U > 0$  and  $U < 0$ . In line with Yang's criterion for the off-diagonal-long-range order (ODLRO) [1], we find that both the maxima and the minima of the correlation function along the antidiagonal scale the same way with  $N$ . Indeed, in the presence of quasi-ODLRO the momentum correlator is dominated by the pair-pair

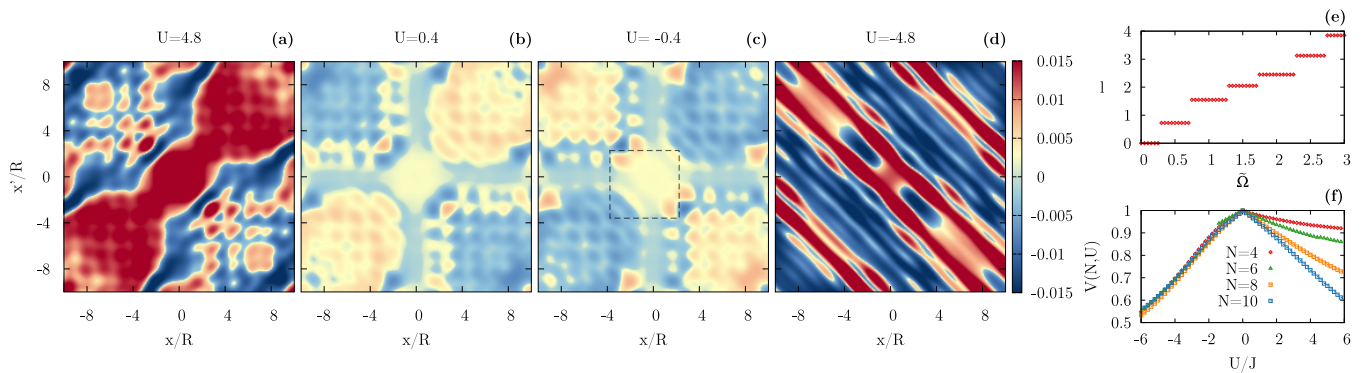


FIG. 3. Long times density-density correlator  $G_{\uparrow,\downarrow}(\mathbf{r}, \mathbf{r}'; t_{exp})$ . The correlation for  $\mathbf{r} = (x, 0)$ ,  $\mathbf{r}' = (x', 0)$  and  $t_{exp} = 100 \omega_0^{-1}$  is evaluated. For weak attractive interaction we observe BCS-like correlations at  $x = -x' \simeq \hbar t_{exp} k_F / m$ . At strong attractive interactions tightly bound pairs are revealed by the enhancement of the correlations along the whole  $x = -x'$  diagonal. In the third panel, the square indicates the size of the Fermi sphere at  $x, x' = \pm \hbar t_{exp} k_F$ . The last two panels are evaluated for a lattice of  $N_s = 10$  sites. We show respectively the quantized shift of the anti-diagonal in the  $(x, x')$  plane as a function of the flux for  $N = 6$  and  $U/J = -5.4$  and the visibility of the anti-diagonal itself for various values of number of particles and interactions. The visibility is defined as  $V(N, U) = \frac{\text{Max}[G_{\uparrow,\downarrow}(x, -x; t)] - \text{Min}[G_{\uparrow,\downarrow}(x, -x; t)]}{\text{Max}[G_{\uparrow,\downarrow}(x, -x; t)] + \text{Min}[G_{\uparrow,\downarrow}(x, -x; t)]}$ . We observe a markedly different  $N$  scaling for repulsive or attractive interactions. The calculations are performed using the DMRG method with  $N = 14$  and  $N_s = 20$ .

correlations, and scales as  $N^\alpha$  with  $0 < \alpha < 1$  for any wavevector  $k$  (See Supplementary Material). For  $U > 0$ , instead the minima of the correlation functions result to be  $\propto N$  and the maxima display weak  $N$ -dependence. As a result, the visibility  $V(N, U)$  presented in Fig. 3, is independent of  $N$  for  $U < 0$  and decreasing with  $N$  for  $U > 0$ . We note that the property clearly emerges already at small  $N$ , this providing a further evidence that ring geometries are well suited for minimizing finite size effects[43].

**Conclusions.** In this work, we demonstrated how the interplay between the particle's phase coherence and the many-body quantum phase coherence of an interacting Fermi gas can be probed with a single protocol: a ring-shaped degenerate gas co-expands with a second free Fermi gas providing the reference for the phase. Despite the logic of the protocol is identical to the one applied to bosonic rings, the results are markedly different from the bosonic case. We described the ring-shaped gas through the Hubbard model with the local interaction  $U$  ranging from positive to negative values. We analysed the density-density correlators. Such quantity can be accessed, for example, in cold atoms quantum technology through state of the art processing of the particles density expansion dynamics. In particular, we note that also continuous ring-shape (no lattice) degenerate gases can be accessed by our theory in the dilute lattice limit (see Supplementary material). For our protocol, we demonstrated that particle's phase information emerges in the intermediate times interference of the expansion; the many-body phase coherence can be tracked at longer times.

*i) Intermediate time expansion.* For Fermi systems the effective magnetic flux imparts the phase winding on a broad momentum distribution. As a result, the relevant information of the phase of fermionic particles needs to be traced in the response of orbitals. This analysis can be carried out in our protocol by suitably subtracting the correlations of non-interacting Fermi gas from the total correlations - Fig.2. As remarkable spin-off of our analysis on the single orbital interference, we note that our results grant the access to the number of particles  $N_\uparrow(N_\downarrow)$ , which is a quantity notoriously hard to observe in cold atoms experiments. The prescription is pretty simple: the number of dislocations obtained in our interferogram Fig.3d are just  $N_\alpha - 1$  with  $\alpha = \uparrow$  or  $\downarrow$ .

*ii) Long time expansion.* For repulsive interactions, we found that the resulting long time image displays enhanced correlations along the diagonal  $k = k'$  reflecting the magnetic correlations. By the application of the effective magnetic flux, the position of the peaks results to be displaced in discrete steps, reflecting the quantized circulation of current along the ring. For attractive interactions a clear broad anti-diagonal  $k = -k'$  surfaces in the expansion. Such feature emerges at  $k = k_F$  because of the fermionic pairing, leading to a many-body quantum coherence of the BCS type [29, 42] (see Supplemental material). We find that anti-diagonal correlations arise also for strong attraction in which the pairs are tightly bound; in this case the peaks dissolve on a broad interval of  $k$ . As the counterpart of the effect found for repelling fermions, the position of the anti-diagonal results to be displaced by the effective magnetic flux in a quantized fashion. The quantitative analysis shows that for repul-

sive/attractive interactions the anti-diagonal correlations resurfacing is characterized by a markedly different dependence on the number of particles. Such effect reflects the Yang's off-diagonal-long-range order scaling of the two-body correlation matrix.

With our work, we bring conceptually relevant aspects of many-body physics to the domain of what can be tested. Our analysis is timely with the current stage of cold atoms experimental advances [44].

*Acknowledgements* We thank T. Haug and C. Salomon for discussions. The Grenoble LANEF framework ANR-10-LABX-51-01 are acknowledged for their support with mutualized infrastructure.

- 
- [1] C. N. Yang, *Rev. Mod. Phys.* **34**, 694 (1962).
- [2] Y. Imry, *Introduction to mesoscopic physics*, 2 (Oxford University Press on Demand, 2002).
- [3] A. Bleszynski-Jayich, W. Shanks, B. Peaudecerf, E. Ginossar, F. Von Oppen, L. Glazman, and J. Harris, *Science* **326**, 272 (2009).
- [4] M. Tinkham, *Introduction to superconductivity* (Courier Corporation, 2004).
- [5] A. J. Leggett *et al.*, *Quantum liquids: Bose condensation and Cooper pairing in condensed-matter systems* (Oxford university press, 2006).
- [6] M. Andrews, C. Townsend, H.-J. Miesner, D. Durfee, D. Kurn, and W. Ketterle, *Science* **275**, 637 (1997).
- [7] Y. Castin and J. Dalibard, *Phys. Rev. A* **55**, 4330 (1997).
- [8] M. Lewenstein and L. You, *Phys. Rev. Lett.* **77**, 3489 (1996).
- [9] H. Kurkjian, Y. Castin, and A. Sinatra, *Phys. Rev. A* **88**, 063623 (2013).
- [10] M. Albiez, R. Gati, J. Fölling, S. Hunsmann, M. Cristiani, and M. K. Oberthaler, *Phys. Rev. Lett.* **95**, 010402 (2005).
- [11] S. Levy, E. Lahoud, I. Shomroni, and J. Steinhauer, *Nature* **449**, 579 (2007).
- [12] F. Cataliotti, S. Burger, C. Fort, P. Maddaloni, F. Minardi, A. Trombettoni, A. Smerzi, and M. Inguscio, *Science* **293**, 843 (2001).
- [13] A. Smerzi, S. Fantoni, S. Giovanazzi, and S. Shenoy, *Phys. Rev. Lett.* **79**, 4950 (1997).
- [14] M. Inguscio, W. Ketterle, and C. Salomon, *Ultra-cold Fermi Gases: Proceedings of the International School of Physics " Enrico Fermi", Course CLXIV, [held In] Varenna on Lake Como, Villa Monastero, 20-30 June 2006*, Vol. 164 (IOS press, 2007).
- [15] P. Massignan, M. Zaccanti, and G. M. Bruun, *Reports on Progress in Physics* **77**, 034401 (2014).
- [16] A. Amico, F. Scazza, G. Valtolina, P. E. S. Tavares, W. Ketterle, M. Inguscio, G. Roati, and M. Zaccanti, *Phys. Rev. Lett.* **121**, 253602 (2018).
- [17] G. C. Strinati, P. Pieri, G. Röpke, P. Schuck, and M. Urban, *Phys. Rep.* **738**, 1 (2018).
- [18] G. Valtolina, A. Burchianti, A. Amico, E. Neri, K. Khani, J. A. Seman, A. Trombettoni, A. Smerzi, M. Zaccanti, M. Inguscio, *et al.*, *Science* **350**, 1505 (2015).
- [19] W. Kwon, G. Del Pace, R. Panza, M. Inguscio, W. Zwerger, M. Zaccanti, F. Scazza, and G. Roati, *Science* **369**, 84 (2020).
- [20] N. Luick, L. Sobirey, M. Bohlen, V. P. Singh, L. Mathey, T. Lompe, and H. Moritz, *Science* **369**, 89 (2020).
- [21] S. Eckel, F. Jendrzejewski, A. Kumar, C. J. Lobb, and G. K. Campbell, *Phys. Rev. X* **4**, 031052 (2014).
- [22] L. Corman, L. Chomaz, T. Bienaimé, R. Desbuquois, C. Weitenberg, S. Nascimbene, J. Dalibard, and J. Beugnon, *Phys. Rev. Lett.* **113**, 135302 (2014).
- [23] R. Mathew, A. Kumar, S. Eckel, F. Jendrzejewski, G. K. Campbell, M. Edwards, and E. Tiesinga, *Phys. Rev. A* **92**, 033602 (2015).
- [24] L. Amico, M. Boshier, G. Birkel, A. Minguzzi, C. Miniatura, L. C. Kwek, D. Aghamalyan, V. Ahufinger, N. Andrei, A. S. Arnold, M. Baker, T. A. Bell, T. Bland, J. P. Brantut, D. Cassettari, *et al.*, *State of the art and perspective on atomtronics* (2020), arXiv:2008.04439 [cond-mat.quant-gas].
- [25] T. Roscilde, M. F. Faulkner, S. T. Bramwell, and P. C. Holdsworth, *New Journal of Physics* **18**, 075003 (2016).
- [26] P. Naldesi, J. P. Gomez, V. Dunjko, H. Perrin, M. Olshanii, L. Amico, and A. Minguzzi, *Enhancing sensitivity to rotations with quantum solitonic currents* (2020), arXiv:1901.09398 [cond-mat.quant-gas].
- [27] P. Naldesi, J. P. Gomez, B. Malomed, M. Olshanii, A. Minguzzi, and L. Amico, *Phys. Rev. Lett.* **122**, 053001 (2019).
- [28] W. Belzig, C. Schroll, and C. Bruder, *Phys. Rev. A* **75**, 063611 (2007).
- [29] S. Staudenmayer, W. Belzig, and C. Bruder, *Phys. Rev. A* **77**, 013612 (2008).
- [30] J. Dalibard, F. Gerbier, G. Juzeliūnas, and P. Öhberg, *Rev. Mod. Phys.* **83**, 1523 (2011).
- [31] N. Andrei, *Low-Dimensional Quantum Field Theories for Condensed Matter Physicists* (World Scientific Publishing Co, 2013) pp , 457 (1995).
- [32] J. N. Fuchs, A. Recati, and W. Zwerger, *Phys. Rev. Lett.* **93**, 090408 (2004).
- [33] F. Marsiglio, *Phys. Rev. B* **55**, 575 (1997).
- [34] X.-W. Guan, M. T. Batchelor, and C. Lee, *Reviews of Modern Physics* **85**, 1633 (2013).
- [35] L. Amico, A. Osterloh, and F. Cataliotti, *Phys. Rev. Lett.* **95**, 063201 (2005).
- [36] G. Pecci, P. Naldesi, L. Amico, and A. Minguzzi, arXiv preprint arXiv:2010.03552 (2020).
- [37] T. Haug, J. Tan, M. Theng, R. Dumke, L.-C. Kwek, and L. Amico, *Phys. Rev. A* **97**, 013633 (2018).
- [38] S. Moulder, S. Beattie, R. P. Smith, N. Tammuz, and Z. Hadzibabic, *Phys. Rev. A* **86**, 013629 (2012).
- [39] K. C. Wright, R. B. Blakestad, C. J. Lobb, W. D. Phillips, and G. K. Campbell, *Phys. Rev. A* **88**, 063633 (2013).
- [40] K. C. Wright, R. B. Blakestad, C. J. Lobb, W. D. Phillips, and G. K. Campbell, *Phys. Rev. Lett.* **110**, 025302 (2013).
- [41] H. Tasaki, *Physics and mathematics of quantum many-body systems* (Springer, 2020).
- [42] E. Altman, E. Demler, and M. D. Lukin, *Phys. Rev. A* **70**, 013603 (2004).
- [43] M. E. Fisher and M. N. Barber, *Phys. Rev. Lett.* **28**, 1516 (1972).
- [44] Y. Cai, D. G. Allman, P. Sabharwal, and K. C. Wright, arXiv preprint arXiv:2104.02218 (2021).
- [45] F. H. Essler, H. Frahm, F. Göhmann, A. Klümper, and V. E. Korepin, *The one-dimensional Hubbard model*

(Cambridge University Press, 2005).

- [46] L. Amico and V. Korepin, *Annals of Physics* **314**, 496 (2004).  
 [47] A. Colcelli, G. Mussardo, and A. Trombettoni, *EPL (Europhysics Letters)* **122**, 50006 (2018).

### Free fermion gas

In this section we show the analytical results for the case  $U = 0$ . In particular, we are interested in evaluating

$$G(\mathbf{r}, \mathbf{r}', t) = \sum_{k,j,n,m=0}^{N_s} w_k^*(\mathbf{r}, t) w_j(\mathbf{r}, t) w_n^*(\mathbf{r}', t) w_m(\mathbf{r}', t) \times \langle c_i^\dagger c_j c_n^\dagger c_m \rangle, \quad (3)$$

where  $c_i$  and  $c_i^\dagger$  are the fermionic annihilation and creation operators and we have indicated by  $i = 0$  the central site. It should be noted that, since in the following we will consider just one spin species, we dropped the indexes  $\uparrow, \downarrow$ . The Wannier functions  $w_j(\mathbf{r})$  are defined as:

$$w_j(\mathbf{r}, t) = \frac{1}{\sqrt{\pi}\sigma} \frac{1}{(1 + i\omega_0 t)} \exp\left\{-\frac{(\mathbf{r} - \mathbf{r}_j)^2}{2\sigma^2(1 + i\omega_0 t)}\right\} \quad (4)$$

where  $\sigma = \sqrt{\hbar/m\omega_0}$  and  $\mathbf{r}_j$  are the initial width and the center of the  $j$ -th Wannier function respectively,  $\omega_0$  being the frequency of the bottom of each lattice well in the harmonic approximation. Imposing that the center and the ring are totally decoupled, the only terms surviving in (3) are:

$$\begin{aligned} \langle n(\mathbf{r}, t) n(\mathbf{r}', t) \rangle &= \langle n(\mathbf{r}, t) n(\mathbf{r}', t) \rangle_{\text{ring}} \\ &+ \sum_{k,j}^{N_s} w_0^*(\mathbf{r}, t) w_j(\mathbf{r}, t) w_k^*(\mathbf{r}', t) w_0(\mathbf{r}', t) (\delta_{kj} - \langle c_k^\dagger c_j \rangle), \end{aligned} \quad (5)$$

where we used the relation  $\langle c_0^\dagger c_0 \rangle = 1$  and we dropped the constant contribution due to the density of the central site. The interference between the two sub-systems is encoded in the second term, while the first one represents the correlations among the particles of the ring.

In order to enhance the visibility of the spiral interferograms, in the following we subtract the term depending on the Kronecker delta:

$$\tilde{G}_0(\mathbf{r}, \mathbf{r}', t) = \sum_{k,j}^{N_s} w_0^*(\mathbf{r}, t) w_j(\mathbf{r}, t) w_k^*(\mathbf{r}', t) w_0(\mathbf{r}', t) \delta_{kj} \quad (6)$$

Remarkably, such expression represents the expectation value of the one-body density matrix of a non-interacting Fermi gas for a completely filled lattice, when the hopping between different sites is inhibited by the Pauli principle and it forms a band insulator. By measuring the

correlation at such filling, one can obtain this term. In alternative, the knowledge of the lattice properties allows to theoretically evaluate it. The one-body correlator  $\langle c_k^\dagger c_j \rangle$  can be determined by solving the non-interacting Schroedinger equation under periodic boundary conditions. An explicit calculation yields:

$$\langle c_k^\dagger c_j \rangle = \sum_{\{n\}} e^{-i\frac{2\pi}{N_s}(j-k)n}, \quad (7)$$

where  $\{n\}$  is the set of integer quantum numbers labelling the energy levels of the Fermi sphere, whose value depends on the applied flux  $\Omega$ .

Hence, the relevant noise correlator for spiral interferograms reads:

$$\begin{aligned} \tilde{G}(\mathbf{r}, \mathbf{r}', t) &= -\tilde{G}_0(\mathbf{r}, \mathbf{r}', t) + \sum_{\rho, \sigma = \uparrow, \downarrow} [\langle n_\rho(\mathbf{r}, t) n_\sigma(\mathbf{r}', t) \rangle \\ &- \langle n_\rho(\mathbf{r}, t) \rangle_{\text{ring}} \langle n_\sigma(\mathbf{r}', t) \rangle_{\text{C}} - \langle n_\rho(\mathbf{r}, t) \rangle_{\text{C}} \langle n_\sigma(\mathbf{r}', t) \rangle_{\text{ring}} \\ &- \langle n_\rho(\mathbf{r}, t) n_\sigma(\mathbf{r}', t) \rangle_{\text{ring}} - \langle n_\rho(\mathbf{r}, t) n_\sigma(\mathbf{r}', t) \rangle_{\text{C}}] \end{aligned} \quad (8)$$

Next, we suitably recast Eq. (4), splitting the Gaussian contribution of the modulus from the dynamical phase of the function.

$$\begin{aligned} \tilde{G}(\mathbf{r}, \mathbf{r}', t) &= \\ &= -|A(t)|^4 e^{-\frac{\sigma^2}{2b^2(t)}(r^2+r'^2)} e^{-i\frac{\hbar t}{mb^2(t)}(r^2-r'^2)} \\ &\times \sum_{kj} e^{-\frac{1}{2\sigma^2 b^2(t)}((r-r_j)^2+(r'-r_k)^2)} e^{i\frac{\hbar t}{mb^2(t)}((r-r_j)^2-(r'-r_k)^2)} \\ &\times \sum_{\{n\}} e^{-i\frac{2\pi}{N_s}(j-k)n} \equiv -\sum_{\{n\}} I_n(\mathbf{r}) I_n^*(\mathbf{r}') \end{aligned} \quad (9)$$

where  $b(t) = \sqrt{1 + \omega_0^2 t^2}$  and  $A(t)$  is the complex time-dependent amplitude of the Wannier functions. In the last equivalence we separate the summation over the two indexes: once  $r'$  is fixed, Eq. (9) will be a superposition of single-orbital functions  $I_n(r)$ , each weighted with a  $n$ -dependent coefficient. We show explicitly in Fig. 2 the full correlator and the single-orbital contributions for different number of particles. We also make a comparison with the non interacting bosonic case, where, for fixed  $n$ , the full correlator is proportional to the function  $I_n(\mathbf{r}) I_n^*(\mathbf{r}')$ , yielding a perfect spiral interference pattern whose number of branches is equal to  $n$ .

### Time of flight

We now focus on the momentum distribution of the particles on the ring, that can be addressed through time of flight imaging using the same protocol proposed in the main text. Such observable can be measured by looking at the density distribution of the gas after the expansion for large values of  $t$ . Indeed by taking the limit  $t \rightarrow \infty$  in Eq.(4), one gets  $w_j(\mathbf{r}, t) \propto e^{i\mathbf{k}(\mathbf{r}) \cdot \mathbf{r}_j}$  where  $\mathbf{k}(\mathbf{r}) =$

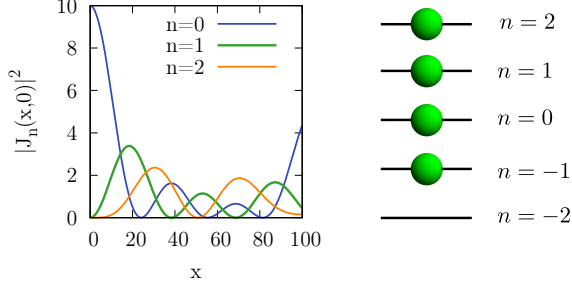


FIG. 4. On the left, profile  $|J_n(x,0)|^2$  for different  $n$ . We see that when  $n = 0$  the function has a finite value in the origin  $x = y = 0$ . As  $n$  increases, the function collapses to zero in this point. On the right, we show the configuration of the quantum numbers for  $N = 4$  spinless fermions. In the ground state, they are selected in order to minimize the value of the current.

$\frac{m_s}{\hbar t} \mathbf{r}$ . Hence, one has  $\lim_{t \rightarrow \infty} \langle n(\mathbf{r}, t) \rangle \propto \langle n(\mathbf{k}) \rangle$ , where the momentum distribution is defined as

$$\langle n(\mathbf{k}) \rangle \propto \sum_{i,j} e^{i\mathbf{k} \cdot (\mathbf{r}_i - \mathbf{r}_j)} \langle c_i^\dagger c_j \rangle \quad (10)$$

where  $\mathbf{r}_i$  and  $\mathbf{r}_j$  are the position of the lattice sites  $i$  and  $j$ . Using the one-body correlation function evaluated in Eq. (7), one gets:

$$\langle n(\mathbf{k}) \rangle \propto \frac{1}{N_s} \sum_{j=1}^{N_s} \sum_{\{n\}} |e^{iR(k_x \cos \theta_j + k_y \sin \theta_j)} e^{\frac{2\pi i}{N_s} j n}|^2 \quad (11)$$

where we introduced  $(R, \theta_j)$  as the polar coordinates of the  $j$ -th site of the ring and decompose  $\mathbf{k} = (k_x, k_y)$ . Remarkably,  $\theta_j = \frac{2\pi}{N_s} j$ , thus setting  $J_n(x, y) \doteq \sum_{j=1}^{N_s} e^{iR(k_x \cos(\frac{2\pi}{N_s} j) + k_y \sin(\frac{2\pi}{N_s} j))} e^{\frac{2\pi i}{N_s} j n}$  the previous expression can be further simplified:

$$\langle n(\mathbf{k}) \rangle \propto \frac{1}{N_s} \sum_{\{n\}} |J_n(k_x, k_y)|^2. \quad (12)$$

The functions  $J_n(x, y)$  provide the discrete version of the Bessel function of order  $n$ . A remarkable property of such function is that  $|J_n(x, y)|^2$  is non-zero in the origin only when  $n = 0$ , as shown in Fig.4.

From this expression it is evident that the structure of the momentum distribution strongly depends on the set of quantum numbers  $\{n\}$  and therefore on the flux acting on the system. In particular, in the ground state and for  $\tilde{\Omega} = 0$  such numbers are integers selected in order to minimize the current quantum number  $l = \sum_{\{n\}} n$ . Therefore, in this case, the quantum numbers  $n$  are symmetrically disposed around  $n = 0$ , as shown in the example for  $N = 4$  in the right panel of Fig.4.

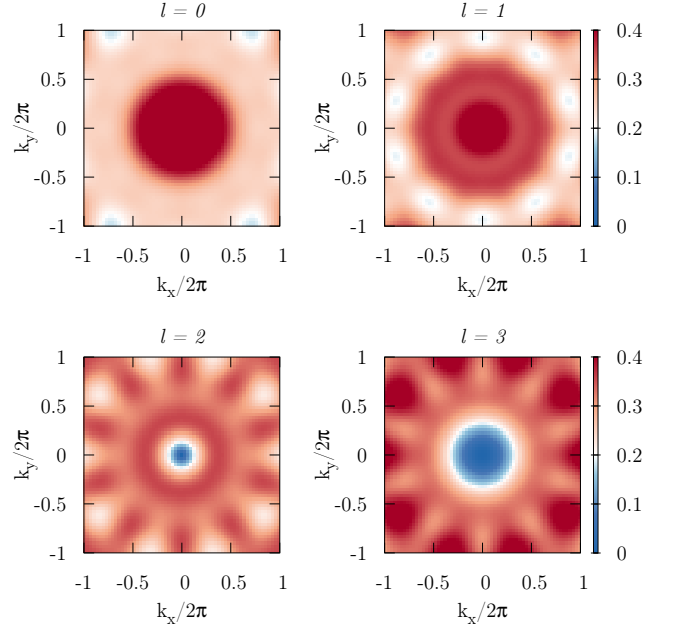


FIG. 5. Time of flight for  $N = 4$  non interacting fermions on  $N_s = 10$  sites. We observe the central peak to disappear when  $l \geq 2$  ie after a shift in the energy levels equal to half of the size of the Fermi sphere.

The momentum distribution for fermions on a lattice at  $\Omega/\Omega_0 = 0$  is expected to show a peak in the center  $k_x = k_y = 0$ , that disappears for large values of flux [35].

In order to observe a collapse of the momentum distribution for  $k_x = k_y = 0$ , we have to excite all the energy levels of the Fermi sphere until  $n = 0$  and correspondingly  $J_0(k_x, k_y)$  are excluded from the summation in Eq.(12). This is achieved after a shift in the energy levels equal to the half of the size of the Fermi sphere, as we show in Fig.5 for  $N = 4$  particles.

### Continuous limit of the Hubbard rings

We sketch the derivation of the Gaudin-Yang model as continuous limit of the Hubbard quantum dynamics (here, we put  $\Omega = 0$ ).

Let's define the density of fermions in the lattice as  $D = N/(N_s \Delta)$ ,  $\Delta$  being the lattice spacing. In the continuous limit  $\Delta \rightarrow 0$ , which implies that the filling factor  $\nu = N/N_s = D\Delta$  must be accordingly small. In the continuous limit the fermionic operators must be rescaled:  $c_{i,\sigma} = \sqrt{\Delta} \Psi_\sigma(x)$ ,  $n_{i,\sigma} = \Delta \Psi_\sigma^\dagger(x) \Psi_\sigma(x)$ ,  $x = \Delta i$ . Then, the Hubbard model reduces to the Fermi gas quantum field theory:  $\mathcal{H}_{FH} = J\Delta^2 \mathcal{H}_{FG} - 2N$ ,  $\mathcal{H}_{FG} = \int dx [(\partial_x \Psi_\sigma^\dagger)(\partial_x \Psi_\sigma) + c \Psi_\sigma^\dagger \Psi_\sigma^\dagger \Psi_\sigma \Psi_\sigma]$ , with  $c = U/(J\Delta)$ . The quantum fields obey  $\{\Psi_\sigma(x), \Psi_{\sigma'}^\dagger(y)\} = \delta_{\sigma,\sigma'} \delta(x - y)$  and  $\{\Psi_\sigma^\dagger(x), \Psi_{\sigma'}^\dagger(y)\} = 0$ . The Fermi

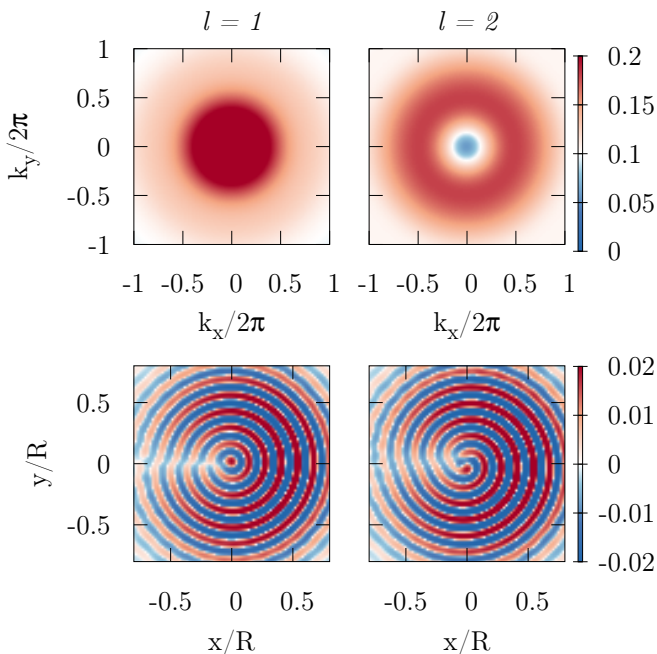


FIG. 6. Time of flight (top) and  $\tilde{G}^{(C,R)}$  (bottom) for a dilute system of  $N = 4$  particle on  $N_s = 30$  sites for various values of angular momentum (left panels  $l = 1$ , right panels  $l = 2$ ). We consider here a repulsive interaction  $U/J = 2$ . Consistently with the text, in the bottom plots we observe  $N_{\uparrow} - 1$  dislocations.

gas field theory is the quantum field theory for the Gaudin-Yang model. Such statement can be demonstrated by writing the eigenstates of  $\mathcal{H}_{FG}$  as  $|\psi(\lambda)\rangle = \int d\mathbf{z} \chi(\mathbf{z}|\lambda) \Psi_{\sigma}^{\dagger}(z_1) \dots \Psi_{\sigma}^{\dagger}(z_N) |0\rangle$ . Then, it can be proved that  $\chi(\mathbf{z}|\lambda)$  must be eigenfunctions of the Gaudin-Yang Hamiltonian

$$H_{G-Y} = - \sum_{j=1}^{N_s} \frac{\partial^2}{\partial z_j^2} - 2c \sum_{N_s \geq j > k \geq 1} \delta(z_j - z_k). \quad (13)$$

Both the Hubbard and the Gaudin-Yang models are integrable by Bethe Ansatz[45]. This should be contrasted with the bosonic case, in which the lattice regularization can spoil the integrability of the continuous theory[46].

The mapping sketched above makes our results for dilute lattices applicable to a 1d fermionic gas with delta-interaction. In Fig.6 we show the time of flight and the interference term  $\tilde{G}^{(C,R)}$  at intermediate times for a dilute systems of  $N = 4$  particles on  $N_s = 30$  sites for  $U = 2$ . We observe the characteristic hole in the center of the momentum distribution due to the action of the flux, as described in the previous section for non-interacting fermions. Furthermore, in the second line, we recognize a dislocated spiral-like interference pattern, carrying information about the angular momentum of the system and marking the fermionic nature of the particles.

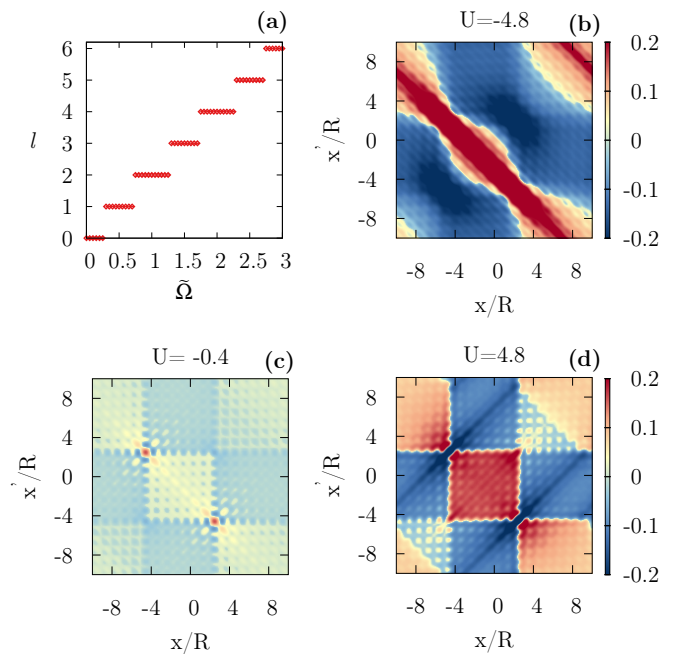


FIG. 7. The panel (a) shows the shift of the antidiagonal  $x = -x'$  as a function of the applied flux  $\tilde{\Omega}$  for  $U/J = -5.4$ . In the panels (b), (c), (d), we show the one dimensional correlator  $G_{\uparrow,\downarrow}^{(1d)}(x, x'; t)$  Eq. 14 at long expansion time  $t_{exp}$  and with flux  $\tilde{\Omega} = 1.4$ . We observe that similar structures as in the two dimensional case emerge. The peaks surfacing at  $U = 0.4$  are located at  $k = \pm k_F$ . The figure refers to a system of  $N = 14$  and  $N_s = 20$ .

### One-dimensional correlations

In this section, we study the correlation function in a 1d system in the reciprocal space. We shall see that we such correlations display similar features of the noise correlations in the time-of-flight momentum distribution. The correlation functions reads

$$G_{\uparrow,\downarrow}^{(1d)}(x, x'; t) \propto \sum_{l,j,m,n}^{N_s} e^{i\frac{x}{R}(l-j) + i\frac{x'}{R}(m-n)} \langle c_{l,\uparrow}^{\dagger} c_{j,\uparrow} c_{m,\downarrow}^{\dagger} c_{n,\downarrow} \rangle \quad (14)$$

where the indexes  $i, j, l, m$  label the sites of the chain and  $R = 2\pi L$  is the radius of the ring,  $L$  being the length of the chain. Remarkably, the correlation matrix  $\langle c_{l,\uparrow}^{\dagger} c_{j,\uparrow} c_{m,\downarrow}^{\dagger} c_{n,\downarrow} \rangle$  is the same as the one used in the main text. We see in Fig.7 that such correlator carries the same information as the two-dimensional one, with a peak along the anti-diagonal  $x = -x'$  for negative  $U$  revealing the formation of BCS-like pairs in the system. Because of the different geometry of the system with respect to the two-dimensional case, we observe a symmetry breaking along the diagonal  $x = x'$  for non-zero flux. This is represented by a unidirectional shift of the anti-diagonal as a function of the flux that, as shown in Fig.7, is still occurring in quantized steps.

The connection between BCS pairing and the peaks along the antidiagonal of the noise correlator descends from the general expression of the BCS ground state. Consider indeed the  $|BCS\rangle = \prod_k (u_k + v_k b_{k,\uparrow}^\dagger b_{-k,\downarrow}^\dagger) |0\rangle$ , where  $b_{k,\rho}^\dagger$  is the creation operator for a particle with momentum  $k$  and spin  $\rho$  and  $|0\rangle$  is the BCS vacuum. By an explicit calculation we find the noise correlator to be:

$$\sum_{\rho,\sigma} \langle n_\rho(q) n_\sigma(q') \rangle = 2|v_q|^2 |u_{q'}|^2 \left( \delta(q - q') \delta_{\rho,\sigma} + \delta(q + q') (1 - \delta_{\rho,\sigma}) \right) \quad (15)$$

Where the momentum density operator is defined as  $n_\rho(q) = b_{q,\rho}^\dagger b_{q,\rho}$ . From this expression we see that, when  $\rho \neq \sigma$ , this correlation function shows a characteristic peak along  $q = -q'$ , with an envelope mediated by the amplitudes of the BCS state. We can also explicitly study the dependence of such correlator on the flux  $\tilde{\Omega}$ . In order to do so, we introduce the latter using the Peierls substitution on the creation/annihilation operators in the real space ie  $b_{j,\rho} \rightarrow e^{i\tilde{\Omega}j} b_{j,\rho} \doteq \tilde{b}_{j,\rho}$ . The Fourier transform yields  $\tilde{b}_{q,\rho} = \frac{1}{N_s} \sum_{j=1} e^{iqj} \tilde{b}_{j,\rho} = \frac{1}{N_s} \sum_{j=1} e^{i(q+\tilde{\Omega})j} b_{j,\rho} = b_{q+\tilde{\Omega},\rho}$ . Therefore, the Peierls substitution shifts all the momenta of the same flux-dependent amount. Inserting such result in Eq.(15), we don't affect the term proportional to  $\delta_{\rho,\sigma}$ , while the second term, proportional to the peak along  $q = -q'$ , get shifted by a discrete amount  $2\tilde{\Omega}$ .

### Visibility $V(U, N)$ Vs quasi-ODLRO

The concept of off-diagonal long range order allows to quantify uniquely the properties of condensation or pairing in interacting quantum fluids [1]. For paired fermions, such as superconductors and atomic Fermi superfluids, the relevant correlator is the two-body density matrix:  $\rho_2(x, x', y, y') = \langle \psi_\uparrow^\dagger(x) \psi_\downarrow^\dagger(x') \psi_\downarrow(y) \psi_\uparrow(y') \rangle$  quantifying phase coherence between one pair centered at  $X = (x + x')/2$  and a second one at  $Y = (y + y')/2$ . Existence of ODLRO implies that  $\rho_2(x, x', y, y') \simeq \lambda_0(N) \Phi_0^*(x, x') \Phi_0(y, y')$  with  $\Phi_0$  natural orbital of  $\rho_2$

with macroscopic eigenvalue  $\lambda_0 = O(N)$ . Similarly, by analogy with bosonic systems [47], for quasi-ODRLO one expects that quantum fluctuations reduce the scaling to  $\lambda_0(N) = O(N^\alpha)$  with  $0 < \alpha < 1$ . All the above relations are readily generalized to lattice systems, by considering the discretized versions of  $\rho_2$  and  $\Phi_0$  according to  $\rho_2(j, l, m, n) = \langle c_{j,\uparrow}^\dagger c_{l,\downarrow}^\dagger c_{m,\downarrow} c_{n,\uparrow} \rangle$  and  $\Phi_0(j, l) = \Phi_0(x_j, x_l)$ . We show here how the  $G_{\uparrow\downarrow}$  correlator at long times and its visibility allows precisely to address off-diagonal long-range order.

We start by recalling that (see Section on Time of Flight above and [42]) the long-time density correlators yield information on the correlations in momentum space of the gas before expansion:  $\lim_{t \rightarrow \infty} G_{\uparrow\downarrow}(\mathbf{r}, \mathbf{r}', t) \propto \langle n_\uparrow(\mathbf{k}) n_\downarrow(\mathbf{k}') \rangle$  with  $\mathbf{k} = m\mathbf{r}/\hbar t$ , and where the momentum correlations are defined as

$$\langle n_\uparrow(\mathbf{k}) n_\downarrow(\mathbf{k}') \rangle = \sum_{jlmn} e^{i\mathbf{k} \cdot (\mathbf{x}_j - \mathbf{x}_l)} e^{i\mathbf{k}' \cdot (\mathbf{x}_m - \mathbf{x}_n)} \langle c_{j,\uparrow}^\dagger c_{l,\uparrow} c_{m,\downarrow}^\dagger c_{n,\downarrow} \rangle \quad (16)$$

Hence, they are readily related to the two-body density matrix upon commutation of the order of the operators. If (quasi)ODRLO holds, along the antidiagonal  $\mathbf{k}' = -\mathbf{k}$  one has

$$\langle n_\uparrow(\mathbf{k}) n_\downarrow(-\mathbf{k}) \rangle \simeq \lambda_0(N) |\tilde{\Phi}_0(\mathbf{k})|^2 \quad (17)$$

where we have defined  $\tilde{\Phi}_0(\mathbf{k}) = \sum_{j,l} e^{i\mathbf{k} \cdot (\mathbf{r}_j - \mathbf{r}_l)} \Phi_0(j, l)$  and used that  $\Phi_0(j, l)$  is an even function of  $j - l$ .

The connected part of the correlator  $\langle n_\uparrow(\mathbf{k}) n_\downarrow(-\mathbf{k}) \rangle_c$  contains essentially the same information of ODLRO as the full one since no ODRLO is found for fermionic systems in the disconnected terms [1].

Combining all the above considerations, we readily conclude that the visibility of the momentum correlator along the anti-diagonal  $\mathbf{k}' = -\mathbf{k}$ , in presence of quasi-ODLRO is predicted to behave as

$$V(U, N) = \frac{\text{Max}|\tilde{\Phi}_0(\mathbf{k})|^2 - \text{Min}|\tilde{\Phi}_0(\mathbf{k})|^2}{\text{Max}|\tilde{\Phi}_0(\mathbf{k})|^2 + \text{Min}|\tilde{\Phi}_0(\mathbf{k})|^2} \quad (18)$$

ie, noticeably, it is independent on  $N$ .